Ultrafast Superconducting Single-Photon Optical Detectors and Their Applications

Roman Sobolewski, A. Verevkin, G. N. Gol'tsman, A. Lipatov, and K. Wilsher

***Abstract*—We present a new class of ultrafast single-photon detectors for counting both visible and infrared photons. The detection mechanism is based on photon-induced hotspot formation, which forces the supercurrent redistribution and leads to the appearance of a transient resistive barrier across an ultrathin, submicrometer-width, superconducting stripe. The devices were fabricated from 3.5-nm- and 10-nm-thick NbN films, patterned into <200-nm-wide stripes in the 4 × 4-μm^2 or 10 × 10-μm^2 meander-type geometry, and operated at 4.2 K, well below the NbN critical temperature (T_c = 10–11 K). Continuous-wave and pulsed-laser optical sources in the 400-mm-to 3500-nm-wavelength range were used to determine the detector performance in the photon-counting mode. Experimental quantum efficiency was found to exponentially depend on the photon wavelength, and for our best, 3.5-nm-thick, 100-μm^2-area devices varied from >10% for 405-nm radiation to 3.5% for 1550-nm photons. The detector response time and jitter were ∼100 ps and 35 ps, respectively, and were acquisition system limited. The dark counts were below 0.01 per second at optimal biasing. In terms of the counting rate, jitter, and dark counts, the NbN single-photon detectors significantly outperform their semiconductor counterparts. Already-identified applications for our devices range from noncontact testing of semiconductor CMOS VLSI circuits to free-space quantum cryptography and communications.**

***Index Terms*—CMOS testing, nonequilibrium superconductivity, quantum cryptography, single-photon detectors, ultrathin NbN films.**

I. Introduction

SINGLE-PHOTON detectors (SPD's) represent the ultimate sensitivity limit for any quantum radiation detectors. In the visible light range, the best known and most widely used are Si avalanche photodiodes (APD's) [1] and photomultiplier tubes (PMT's) [2]. The operation of photomultiplier/avalanche devices is based on the electron cascade and multiplication effect, which significantly amplifies the response and allows for an easy measurement of the response pulses. Unfortunately, this method of registration leads to a large time lag and jitter of the device response. In addition, the APD's and PMT's counting rates are well below 100 MHz. Their actual speed is even more limited since, for noise reduction purposes, they have to be used in a time-gated mode, which reduces their counting rates to 10 MHz or below.

Detection of single-photon infrared (IR) radiation remains a major technological challenge because IR photons carry significantly less energy than those of visible light, making it difficult to engineer an efficient electron cascade. The most successful Si APD's have their sensitivity restricted by the bandgap, while APD's based on narrow-gap semiconductors exhibit unacceptably large dark counts [3]. The best quantum efficiency (QE) reported for InGaAs APD's is ∼16% at 1.2 μm, but the large, ∼0.5-ns jitter and high, $>10^4$-per-second dark counts [3] make them not attractive for several important applications, including practical quantum communication systems [2], [4]. The PMT's are bulky and demonstrate QE < 0.001% at 1.2 μm and ∼150-ps jitter [2]. Finally, the most recently proposed far-IR detectors based on single-electron transistors [5] are very slow and require millikelvin temperatures.

In this presentation, we review our most recent research on superconducting SPD's (SSPD's). We demonstrate their excellent operating parameters and show that in many areas they drastically outperform their semiconductor counterparts. Applications ranging from visible free-space and IR fiber-based quantum communications [4] to nondestructive testing of very-large-scale-integrated (VLSI) devices [6] require SPD's with very high counting rates, very low jitter, and negligible dark counts. Effective operation in the mid-IR spectrum range is also very important. Our nanostructured, NbN SSPD's [7], [8], based on the nonequilibrium hot-electron effect in ultrathin superconducting films [9], offer picosecond time resolution and jitter, experimental QE ranging from >10% for visible light to 5% to 3% in the 1.3-μm to 1.55-μm IR range, and very low dark counts.

The next section is devoted to an overview of the physics of operation of SSPD's. Section III briefly discusses our fabrication methods, while Section IV presents the experimental results and shows the SSPD performance. Already identified applications of SSPD's for VLSI chip testing and quantum cryptography are reviewed in Section V, and our conclusions, including the direct comparison with other SPD's, are presented in Section VI.

II. Physics of Operation of SSPDs

Superconducting devices have already become practical as radiation sensors because of their quantum nature and low-noise

Manuscript received September 5, 2002. This work was supported by the AFOSR Grant F49620-01-1-0463 (Rochester), by RFBR Grant 02-02-16774 (Moscow), and by NPTest, San Jose, CA USA.

R. Sobolewski is with the Department of Electrical and Computer Engineering and the Laboratory for Laser Energetics, University of Rochester, Rochester, NY 14627 USA, and is also with the Institute of Physics, Polish Academy of Sciences, PL-02668 Warszawa, Poland (e-mail: Sobolewski@ece.rochester.edu).

A. Verevkin is with the Department of Electrical and Computer Engineering and the Laboratory for Laser Energetics, University of Rochester, Rochester, NY 14627 USA.

G. N. Gol'tsman and A. Lipatov are with the Department of Physics, Moscow State Pedagogical University, Moscow 119435, Russia (e-mail: goltsman00@mail.ru).

K. Wilsher is with NPTest, San Jose, CA 95134 USA (e-mail: kwilsher@nptest.com).

Digital Object Identifier 10.1109/TASC.2003.814178

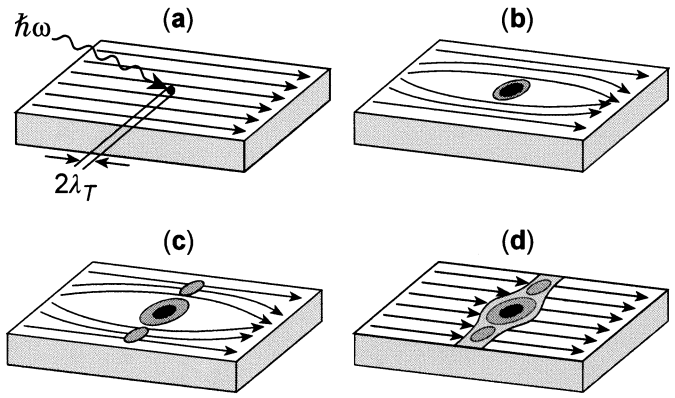

Fig. 1. Schematics of the hot spot-generated and supercurrent-assisted formation of a resistive barrier in an ultrathin and submicrometer-width superconducting stripe, kept at a temperature far below T_c. The arrows indicate the flow direction of a supercurrent biasing the stripe.

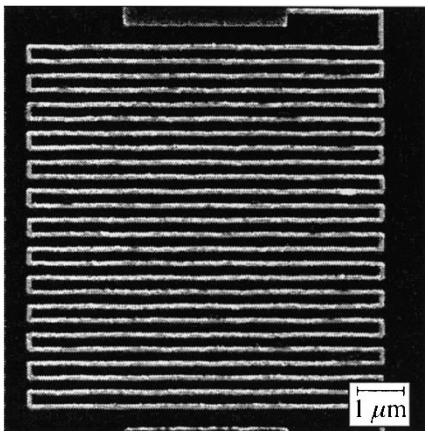

Fig. 2. A scanning-electron-microscope image of a 10×8-μm^2, 10-nm-thick meander-type SSPD. The superconducting stripe width is $\sim$130 nm and $f = 0.2$.

cryogenic operation environment [9]. The superconducting energy gap 2Δ is typically two to three orders of magnitude lower than the gap in semiconductors; thus, individual optical photons are able to generate a large number of excited carriers when hitting a superconductor [10]. Measuring the resulting electrical pulse allows precise detection of the photon arrival. The efficient avalanche also results in an enhanced resolution of energy-resolving devices, such as superconducting tunnel junctions [11], and extends the range of detectable energies well into the IR-range for photodetectors. Finally, energy relaxation time constants of excited electrons in superconductors are in the picosecond range for both the low-temperature [12] and high-temperature [13] superconductors, assuring the gigahertz repetition rates for superconducting photon counters.

Our SSPD consists of a superconducting stripe whose thickness is less than the electron thermalization length. The device is operated at the temperature far below the material critical temperature T_c, in a regime where the bias current I is close to the critical value I_c. Absorption of a photon leads to formation of a hotspot region [14] where superconductivity is suppressed or even destroyed [Fig. 1(a)]. During the initial thermalization, the hotspot grows in size [Fig. 1(b)] as hot electrons diffuse out of the hotspot core. The supercurrent, which biases the device, is expelled from the resistive hotspot volume and is concentrated in the "sidewalks" near the edges of the film [Fig. 1(c)]. If the current density after this redistribution exceeds the critical value outside the hotspot, phase-slip centers are created in the sidewalks, the superconductivity is destroyed, and the resistive barrier is formed across the entire width of the device [Fig. 1(d)], which, in turn, gives rise to a voltage signal with the amplitude proportional to I. The hotspot growth is followed by its healing, due to the relaxation/cooling of excited electrons and their out-diffusion. Thus, after $\sim$30-ps-long quasiparticle relaxation time [12], the hotspot collapses, superconductivity (zero voltage state) is restored, and the detector is ready to register another photon.

The SSPD operation principle outlined above depends directly on the superconductor characteristics, including 2Δ, diffusivity, electron–electron, and electron–phonon interaction times, as well as on the device geometry. Our material-of-choice is NbN, characterized by the picosecond quasiparticle relaxation, and is suitable for photon counting in the $<$0.4-μm- to 3.5-μm-wavelength range. Photons with a wavelength of 1 μm create in a 10-nm-thick NbN stripe a hotspot of $\sim$20-nm diameter [8]. This means that the single-quantum mode of the SSPD operation requires that the width of our NbN superconductive stripe should be 200 nm or narrower.

III. SSPD Fabrication

NbN superconductive films that we use to fabricate our SSPD's have a thickness of 3.5 nm to 10 nm and are deposited on sapphire substrates by do reactive magnetron sputtering in an Ar and N_2 mixture [15]. The films are characterized by $T_c = 10$ to 11 K, the superconductive transition width $\Delta T_c \sim 0.3$ K, and the critical current density, $j_c = 6$ to 7×10^6 A/cm^2 at 4.2 K. To implement a detector, we have chosen meander-type geometry with characteristic sizes ranging from 10×10 μm^2 to 4×4 μm^2 and a filling factor f (the ratio of the area occupied by the superconducting meander to the detector nominal area) up to 0.5. The width of the superconductive stripe varies from 80 nm to 200 nm. Our patterning and etching procedures are presented in detail in a separate paper [15]; here we mention only that fabrication process includes an electron beam lithography, followed by either ion milling through a Ti mask layer or reactive ion etching through a photoresist.

Figs. 2 and 3 present scanning electron microscope images of two SSPD's that are fabricated according to two different patterning procedures described in [15]. Fig. 2 shows a 10×8-μm^2, 10-nm-thick meander device, fabricated using the Ti mask and ion milling. We note that in this technology, although we can fabricate devices with very narrow (0.1 μm to 0.2 μm in width) meander stripes, f is always much lower than 1, as the separation between the lines remains significantly larger than the line width. Fig. 3 presents the center part of our latest-generation, inter-digitated structures with $f = 0.4$–0.5, etched in a 3.5-nm-thick NbN film. Using ultrathin films and direct reactive ion etching, we not only increased f but also drastically reduced our SSPD stripe edge nonuniformities. This latter factor seems

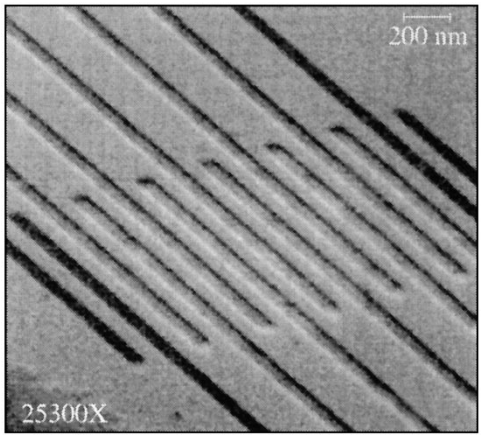

Fig. 3. A scanning-electron-microscope image of an inter-digitated, 3.5-nm-thick SSPD. The width of superconducting stripes (center of the picture) is ~80 nm and $f = 0.5$.

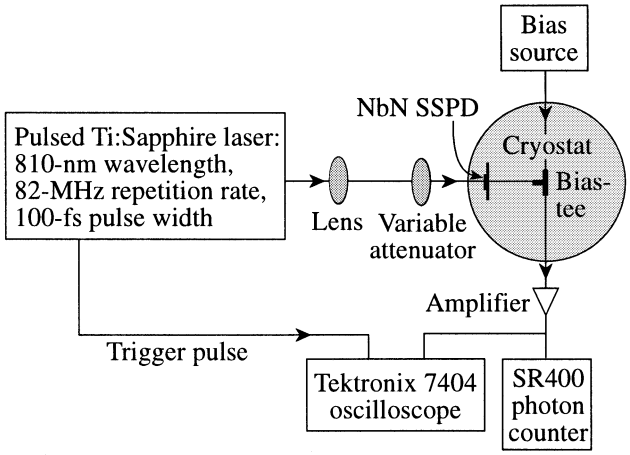

Fig. 4. Experimental setup for a free-space single-photon detection.

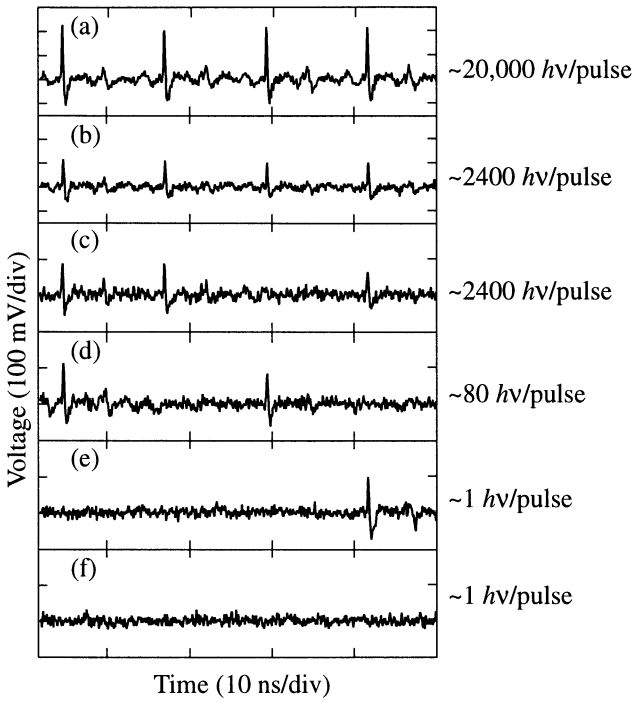

Fig. 5. Real-time responses of a SSPD to trains of 100-fs optical pulses with different numbers of photons per pulse per device area. The presented records illustrate the quantum nature of our device responses at low photon fluxes. Radiation wavelength was 810 nm.

to be dominant in the device performance since, as will be presented later, the 3.5-nm-thick structures exhibited over an order of magnitude higher experimental QE, despite having significantly decreased the photon absorption coefficient η [7].

IV. Experimental Results and the SSPD Performance

A schematic diagram of our experimental setup is shown in Fig. 4. The SSPD was placed on a cold plate inside an optical, liquid-helium cryostat and maintained at 4.2 K. The device was wire-bonded to a microstrip transmission line, and connected to the do bias and rf output circuitry via a broadband, cryogenic bias-tee. The output signal, generated as a result of the photon capture, was amplified by a 20-dB-gain, room-temperature broadband amplifier and either fed into a Tektronix 7404 single-shot digital oscilloscope (synchronously triggered by a Ti : Sapphire laser) or counted by a SR400 photon counter. The room-temperature amplifier and the oscilloscope were characterized by a bandwidth of 0.01 to 12 GHz and 0 to 4 GHz, respectively.

As a photon source, we used 100-fs-wide, 82-MHz-repetition-rate pulses from a self-mode-locked Ti : Sapphire laser. The incident radiation was focused on the device and attenuated to the picowatt level, using banks of neutral density filters. The optical beam diameter was typically ~50 μm to ensure the SSPD uniform illumination. In addition, the QE spectral sensitivity dependence of the SSPD was measured using a continuous-wave (cw) blackbody radiation source and cw and pulsed laser diodes.

Fig. 5 shows a collection of real-time "snapshots" recorded by the single-shot oscilloscope for different numbers of photons per laser pulse, incident on a 4×4-μm^2-area, 10-nm-thick SSPD, and is intended to illustrate the physical response of our devices. Each snapshot presents a 50-ns-long record of the response to four successive 100-fs-wide optical pulses, randomly selected out of a real-time detector output data stream. Trace (a) in Fig. 5 corresponds to essentially a macroscopic signal with ~20 000 photons per pulse hitting the detector. In this case, the device responded to each optical pulse in the laser train. However, as the incident laser intensity was decreased (with other experimental conditions unchanged), the quantum nature of the detector response started to emerge. For ~2400 photons per pulse [traces (b) and (c)], the amplitude of the response pulses was decreased, but, most interestingly, some of the signals were absent in the response train [trace (c)]. Further, over-an-order-of-magnitude decrease in the photon flux did not lead to the decrease of the output signal amplitude, which is characteristic of classical intensity detectors, but many of the response pulses were missing [trace (d)] due to both the limited QE of the device and fluctuations in the number of photons incident on the detector. The quantum nature of our device response was most apparent in the bottom pair of traces: (e) and (f) (1 photon/pulse). We note that in each case, the detector response is very different and its actual performance has to be judged, based on the response averaged over the recording time much longer than 50 ns. We also

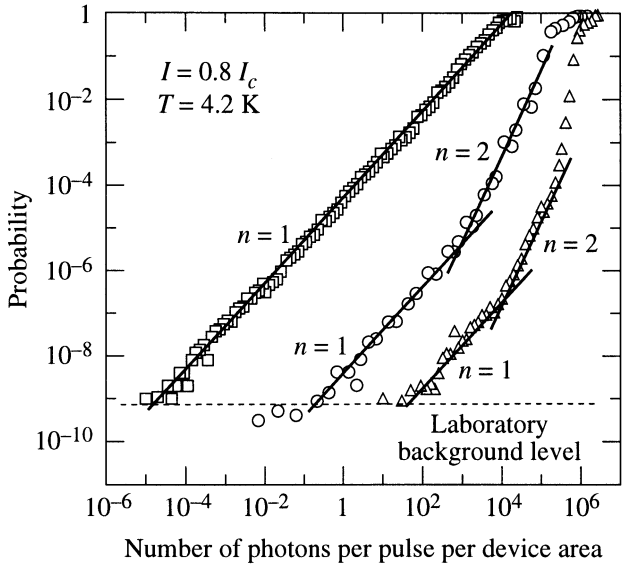

Fig. 6. Probability of photon counting versus the incident photon radiation flux for a 10 × 10-μm^2, 10-nm-thick SSPD at 405-nm (squares), 810-nm (circles), and 1550-nm (triangles) wavelengths. The bias current was $I/I_c = 0.8$ and temperature was 4.2 K. The solid lines illustrate the slope exponents $n = 1$ and $n = 2$.

note that within the time resolution of our electronics, the width of the SSPD response pulses remained constant for all tested photon fluxes.

Records like the ones shown in Fig. 5, but averaged over almost 5×10^9 optical pulses (accumulated over a period of 60 s using the SR400 counter), allowed us to perform statistical analysis of the SSPD response. We observed that for weak photon fluxes (<100 photons per pulse), both the average number of captured pulses for a given photon flux and the signal amplitude remained constant. Fig. 6 shows the probability of photon counting (the ratio of the average number of photons captured per second to the repetition rate of laser pulses) as a function of the average number per pulse of 405-nm, 810-nm, and 1550-nm photons from our Ti : Sapphire laser, incident on a 10 × 10-μ m^2-area, 10-nm-thick device. The device was biased at $I = 0.8I_c$, which was low enough to remain subcritical even when I_c was thermally suppressed at the highest incident light intensities. We note that for 405-nm photons we have a linear dependence over ten orders of magnitude of the photon flux intensity. At wavelength $\lambda = 810$ nm, we observe the linear response at low photon counts and the quadratic law for higher photon fluxes. Finally, for $\lambda = 1550$ nm, the photon counting rate is a highly nonlinear function of the photon flux, with the linear dependence observed only in the range of 10^2–10^4 photons per pulse. We also observe that for the lowest photon fluxes, our experimental data points, for every wavelength, level off at the same $\sim 10^{-9}$ probability value ($\sim$0.1 counts per second). We interpret this response as the laboratory photon background, resulting from accidental photon absorption by our detector. On the other hand, the saturation (probability approaching 1) observed at the highest incident photon flux levels represents the transition of our quantum device into a classical detector [see also Fig. 5(a)].

SSPD's are passive devices and the main sources of dark or false counts are either extrinsic bias-current instabilities or intrinsic fluctuations. The supercurrent fluctuations are dominating at I very close to I_c and rapidly (exponentially) decrease with the I decrease [16], while thermally activated phase-slip centers are typically negligible since we operate our devices at $T \ll T_c$. Thus, long-term stability of I when the detector is biased close to I_c is crucial for minimizing dark counts. One must remember, however, that SSPD's are very broadband sensors and they have to be properly screened from unwanted "photon noise." Large values of dark counts were observed in SSPD implementations, where thermal background radiation from room-temperature objects was inadvertently coupled into the detector [6]. Measurements of dark counts performed in the setup shown in Fig. 4 with the SSPD blocked by a cold load lead to an average of <0.01 counts per second for $I < 0.95I_c$ and were, apparently, limited by our biasing electronics.

The behavior observed in Fig. 6 results from the direct linear dependence of the hotspot size on the photon energy [8]. Thus, for a fixed I, low energy photons generate hotspots too small to ensure efficient SSPD operation, leading to enhanced probability of multiphoton detection with the increase of the photon flux.

For a mean number of m photons per pulse, the probability $P(n)$ of absorbing n photons from a given pulse is given by the Poisson distribution:

$$P(n) \sim \frac{e^{-m}(m)^n}{n!}. \tag{1}$$

For very weak ($m \ll 1$) photon fluxes, the probability of detecting one photon, two photons, three photons, etc., is

$$P(1) \sim m, \quad P(2) \sim \frac{m^2}{2}, \quad P(3) \sim \frac{m^3}{6}, \text{ etc.} \tag{2}$$

Based on (2), we can conclude that for a very low number of photons per pulse incident on the SSPD, we clearly observe in Fig. 6 a single-photon detection regime (exponent $n = 1$) for each studied wavelength. While for 405-nm radiation, the presence of at least one photon in the optical pulse was sufficient to trigger the detector response; for $\lambda = 1550$ nm, the multiphoton absorption ($n \geq 2$) was dominant.

The probability of photon counting measured at the one-photon-per-pulse level incident upon the SSPD and expressed in percents can be defined as its *experimental* QE [more rigorously: detection efficiency (DE)] for a given photon energy. We must stress that QE is a function of I and the highest values are measured for I very close to I_c as shown in [8] and [16]. Typically, we operate our SSPD's with $I \leq 0.95I_c$ since, as we mentioned before, higher I values result in excessive dark counts. Fig. 7 presents experimental QE spectral dependence for two representative 10 × 10-μm^2-area devices. The 3.5-nm-thick SSPD (squares) was an inter-digitated device (see Fig. 3) with 80-nm-wide NbN fingers and $f = 0.5$, while the 10-nm-thick, 200-nm-wide-stripe SSPD (triangles) was a meander-type structure (see Fig. 2) with $f \approx 0.2$. We observe that in both cases, the DE spectral dependence exhibited an exponential, activated-type character with the slope value

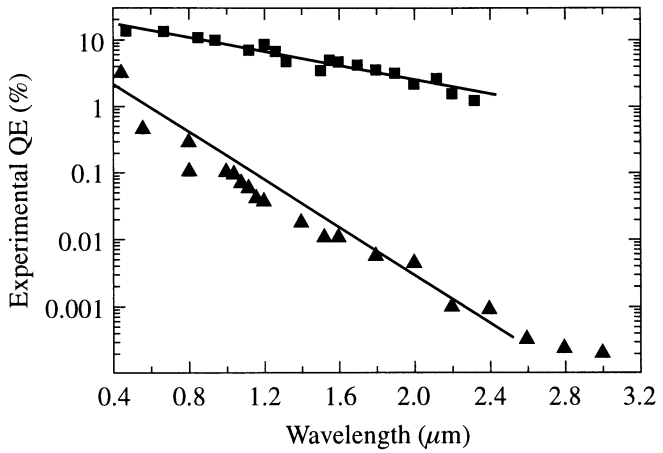

Fig. 7. Spectral dependences of QE for 10 × 10-μm^2 SSPD's, with NbN stripe thickness of 10 nm (triangles) and 3.5 nm (squares), respectively. The solid lines are guides to the eye, illustrating the exponential dependence of the QE on wavelength.

characteristic for all devices with the same thickness [8]. We associate the activation-type behavior with the presence of fluctuations, both extrinsic (stripe width) and intrinsic (superconducting). Simultaneously, we note the drastic improvement in the performance of the 3.5-nm-thick device, as compared to the 10-nm structure, in terms of both the much smaller slope value and the much higher experimental QE [16].

As we mentioned in Section III, this performance improvement is the result of significant improvements in our fabrication technology [15]. The inter-digitated devices implement the ultrathin NbN stripe (larger hotspot dimension) and are truly nanostructured in terms of their physical dimensions. Our best 10-nm-thick SSPD's exhibit experimental QE of $\sim$3% at $\lambda = 405$ nm, decreasing to $\sim$0.01% at $\lambda = 1550$ nm wavelength. At the same time, the 3.5-nm devices reach over an order of magnitude higher QE, ranging from $>$10% at $\lambda = 405$ nm to 3.5% at $\lambda = 1550$ nm.

Proper coupling of our devices to the incident photon flux is another, besides I, limiting factor of the SSPD's experimental QE value. Unlike semiconductor SPD's, the SSPD's have relatively small active area, and only a certain percentage of incident photons is actually absorbed in the ultrathin NbN stripe. The above limitations are extrinsic; thus, in order to estimate the SSPD ultimate performance, defined as the *intrinsic* QE of the superconducting stripe [7], [8], one needs to factor in both the filling factor and the photon absorption coefficient. For 10-nm-thick devices, $f \approx 0.2$ and $\eta \approx 0.3$, leading to the intrinsic QE $=$ DE/$(f\eta)$ and indicate that the possible improvement can reach the factor up to 20. In the case of the 3.5-nm SSPD's, similar calculations indicate that the intrinsic QE should reach the theoretical maximum of 100% for all visible-light wavelengths. The above approach is questionable, however, since for our ultrathin, nanostructured devices, the NbN optical conductivity can be quite different from the do value used in [7, Eq. (1)] to calculate η. The best approach to further increase QE of our detectors is, we believe, not by changing the inter-digitated SSPD geometry, but by adding a backside mirror to reflect the transmitted photons back into the detector. It would be even more effective to form a $\lambda/4$ resonator with the detector acting as one of the resonator mirrors. In this case, however, the SSPD would loose its broadband sensitivity.

Finally, one can define a *system* QE as the number of photons falling at input on the fiber or other coupling optics, divided by the number of photon counts recorded by the detector. This QE definition includes the impact of the detector coupling optics rather than the SSPD size, and it was used in [6] to describe the performance of the early SSPD-based system designed for noninvasive testing of the VLSI chips. The system QE value reported in [6] for one of the first 10-nm-thick, meander-type SSPD's was 0.002% at 1.3-μm wavelength. The latest 3.5-nm devices in the same, fiber-based system (although with significantly modified/improved optics) exhibit the system QE of 2% at the same wavelength, a four-orders-of-magnitude improvement over a two-year period.

We have also performed extensive time-domain characterization of our SSPD's, which are presented in a separate paper [17]. Here we want only to mention that the 10-nm-thick SSPD's have a time resolution $<$100 ps and a device jitter $<$35 ps. Thus, they are able to detect photons with at least 10-Gbit/s counting rate and are more than three orders of magnitude faster than any semiconductor SPD. The 3.5-nm devices are expected to have even better time resolution, reaching the values close to the intrinsic electron-phonon cooling time in ultrathin NbN films of 30 ps [12]. Their jitter has been already measured and is below 20 ps.

V. Applications of SSPDs

A. Noncontact VLSI Chip Testing

Modern high-performance electronic VLSI circuits are extremely difficult to test on both the functional and logic levels because of their complexity, density of packaging, and the use of flip-chip bonding. Devices are increasingly more sensitive and can be easily perturbed during testing, skewing results and slowing the design and development time. Thus, in complex circuits such as microprocessors, nonperturbing methods of testing the chip functionality while it operates are most desirable.

A normally operating silicon CMOS transistor has a nonzero probability of emitting near-IR (0.9 μm to 1.4 μm) photons when current passes through the channel. This is the spontaneous photon emission associated with intea-band transitions as the hot carriers move across the transistor channel [18], [19]. Thus, this photon emission is time-correlated with the transistor switching event and measures directly the transistor switching time, as well as the entire circuit timing characteristics. This intrinsic transistor/circuit information is ideal for timing data acquisition and fault analysis (e.g., leaky transistors tend to emit more photons). The use of near-IR emission from CMOS integrated circuits as a way of diagnosing timing and flaws of VLSI chips has been implemented in the IDS PICA probe system, manufactured by NPTest, San Jose, CA. The IDS PICA system can be equipped with an imaging near-IR detector, the Mepsicron II PMT (Quantar Tech., Inc.) or with the SSPD device [6]. The imaging PMT camera enables light emission from many devices on a test circuit to be simultaneously analyzed, but its IR efficiency is extremely low, leading to hour-long acquisition times and poor noise to signal ratio. The SSPD can analyze

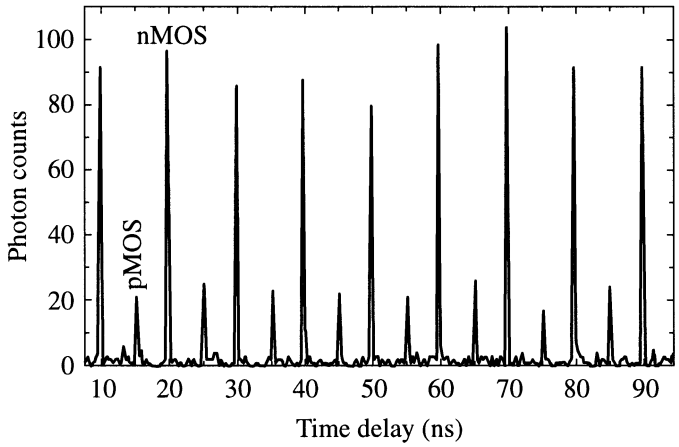

Fig. 8. Histogram of single-photon emissions from a CMOS VLSI chip, collected by the NbN SSPD. Signals from both nMOS and pMOS transistors are clearly visible. The picture was copied directly from the PICA screen.

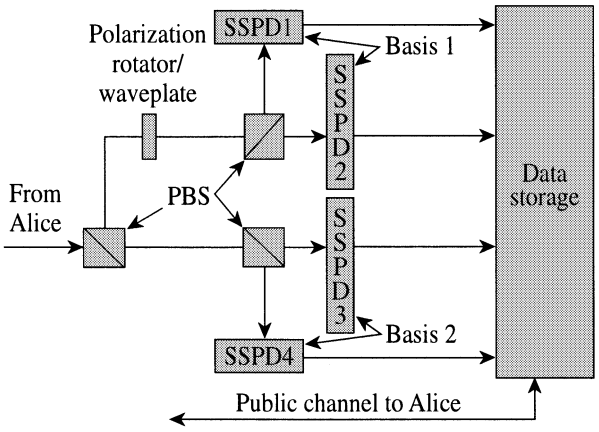

Fig. 9. Quantum cryptography receiver (Bob) based on four NbN SSPD's. PBS stands for polarization beamsplitter.

emission from a single CMOS device only, but its superior IR QE cuts acquisition times to minutes or seconds.

The 3.5-nm-thick NbN SSPD sensors are currently being implemented in the latest IDS PICA version. Test results from a 0.18-μm-linewidth, 1.6-V-bias CMOS integrated circuit running at 100 MHz are shown in Fig. 8. The collected histogram has an extremely high signal-to-noise ratio and the time between transistor switching events can be measured with 10-ps accuracy. In addition to the peaks coming from photon emission from nMOS transistors, we can also observe weak signals collected from pMOS invertors. Holes in pMOS devices have lower mobility and emit IR photons much less frequently. We need to stress that the integrated circuit under test and the photon-collecting microscope are at room temperature and the microscope is connected to the SSPD via a multimode fiber. Physically, the chip-testing apparatus is approximately 2 to 3 m away from the detector, which is placed inside a commercial cryocooler, operating at 3.5 K.

B. Quantum Cryptography

Quantum cryptography (QC) provides a radical improvement over today's methods for secure communications. Unconditionally secret communication is possible in actual physical environments due to the Heisenberg indeterminacy principle: it is impossible to measure the state of a quantum bit without altering it. In QC, the data transport is performed as an exchange of individual photons with their polarization used to code the logic information for the communication protocol. QC is based on the real-time Vernam encryption scheme (so-called "one-time pad") [20]. The quantum key is formed during the photon transmission (there is no pre-existing key), and the Vernam cipher is invulnerable to any computer attack of any strength, including quantum computations.

A recent theoretical paper by Gilbert and Hamrick [21] proves that QC is practical, providing that the data transmission rate is high enough to overcome the intrinsic system losses. Both the transceiver (Alice) and the receiver (Bob) must operate at transmission rates of at least 1 Gbit/s for the practical quantum key distribution operation. A GHz-repetition rate, actively mode-locked laser can be used as the high-speed source of coherent single photons [22], so Alice can readily operate at the GHz range. A serious problem, however, exists at the Bob end, which should count photons not only very efficiently, but also with negligible dark counts and very low jitter.

Fig. 9 presents a possible QC receiver, containing four SSPD's for independent counting of photons with four different polarizations imprinted by Alice. The NbN SSPD's are the most promising for practical QC since, as we have already presented, they exhibit sufficiently high QE and are able to reach GHz range counting rates with very low jitter and negligibly low dark counts. The SSPD's can successfully operate from ultraviolet to IR; thus, they can be implemented in both optical free-space and fiber-based transmission schemes.

TABLE I
PERFORMANCE OF DIFFERENT SPDS OPERATING AT $\lambda = 1.3\ \mu$m

Detector Model	Counting Rate (Hz)	QE (%)	Jitter (ps)	Dark Counts (s^{-1})
InGaAs APD (Fujitsu)	$5.0 \times 10^{6(I)}$	16	200	$500^{(II)}$
IR PMT (Hamamatsu)	9.0×10^{6}	0.5	150	2.0×10^{4}
Si APD (EG&G)	5.0×10^{6}	0.01	350	25
Mepsicron (Quantar, Inc.)	$1.0 \times 10^{6(III)}$	0.001	100	0.1
Superconducting tunnel junction	5.0×10^{3}	60	N/A	N/A
SSPD (measured)	10×10^{9}	5	35	$0.1^{(IV)}$
SSPS (projected)	30×10^{9}	>10	<20	<0.01

(I)Gated regime with 0.1% per gate after-count probability.
(II)Calculated with 10^{-4} per gate probability.
(III)Data for a high-speed version; standard devices exhibit 1×10^{5} s^{-1}.
(IV)Room temperature input.

VI. CONCLUSIONS

Table I presents the main characteristics of our SSPD's, in direct comparison with other modern single-photon detectors.

We compare experimental QE, ultimate counting rate, jitter, and dark counting rates. Our comparison is done for 1.3-μm photons, which is the most-interesting wavelength for applications ranging from noninvasive VLSI chip testing to fiber-based optical communications. As we can see, superconducting detectors significantly outperform even the best semiconductor devices.

ACKNOWLEDGMENT

The authors would like to thank their colleagues from the University of Rochester, Moscow State Pedagogical University, and NPTest for their contributions to the SSPD research.

They are also very grateful to Dr. D. Van Vechten and the U.S. Office of Naval Research for fostering the Rochester-Moscow collaboration.

REFERENCES

[1] T. Isoshima, Y. Isojima, K. Hakomori, K. Kikuchi, K. Nagai, and N. Nakagawa, "Ultrahigh sensitivity single-photon detector using a Si avalanche photodiode for the measurement of ultraweak biochemiluminescence," *Rev. Sci. Instrum.*, vol. 66, pp. 2922–2926, 1995.

[2] A. Karlsson, M. Bourennane, G. Ribordy, H. Zbinden, J. Brendel, J. Rarity, and P. Tapster, "A single-photon counter for long-haul telecom," *IEEE Circuits and Devices Mag.*, vol. 15, pp. 34–40, 1999.

[3] F. Zappa, A. L. Lacaita, S. D. Cova, and P. Lovati, "Solid-state single-photon detectors," *Opt. Eng.*, vol. 35, pp. 938–945, 1996.

[4] A. Verevkin, J. Zhang, W. Slysz, R. Sobolewski, A. Lipatov, O. Okunev, G. Chulkova, A. Korneev, and G. N. Gol'tsman, "Superconducting single-photon detectors for GHz-rate free-space quantum communications," in Free-Space Laser Communication and Laser Imaging, J. C. Ricklin and D. G. Voelz, Eds. Bellingham, WA: SPIE, 2002, vol. 4821, to be published.

[5] O. Astafiev, S. Komiyama, T. Kutsuwa, V. Antonov, Y. Kawaguch, and K. Hirakawa, "Single-photon detector in the microwave range," *Appl. Phys. Lett.*, vol. 80, pp. 4250–4252, 2002.

[6] S. Somani, S. Kasapi, K. Wilsher, W. Lo, R. Sobolewski, and G. Gol'tsman, "New photon detector for device analysis: Superconducting single-photon detector based on a hot electron effect," *J. Vac. Sci. Technol. B, Microelectron. Nanometer Struct.*, vol. 19, pp. 2766–2769, 2001.

[7] G. N. Gol'tsman, O. Okunev, G. Chulkova, A. Lipatov, A. Semenov, K. Smirnov, B. Voronov, A. Dzardanov, C. Williams, and R. Sobolewski, "Picosecond superconducting single-photon optical detector," *Appl. Phys. Lett.*, vol. 79, pp. 705–707, 2001.

[8] A. Verevkin, J. Zhang, R. Sobolewski, A. Lipatov, O. Okunev, G. Chulkova, A. Korneev, K. Smirnov, G. N. Gol'tsman, and A. Semenov, "Detection efficiency of large-active-area NbN single-photon superconducting detectors in the ultraviolet to near-infrared range," *Appl. Phys. Lett.*, vol. 80, pp. 4687–4689, 2002.

[9] A. D. Semenov, G. N. Gol'tsman, and R. Sobolewski, "Hot-electron effect in superconductors and its applications for radiation sensors," *Supercond. Sci. Technol.*, vol. 15, pp. R1–R16, 2002.

[10] K. S. Il'in, I. I. Milosmaya, A. A. Verevkin, G. N. Gol'tsman, E. M. Gershenzon, and R. Sobolewski, "Ultimate quantum efficiency of a superconducting hot-electron photodetector," *Appl. Phys. Lett.*, vol. 73, pp. 3938–3940, 1998.

[11] A. Peacock, P. Verhoeve, N. Rando, A. van Dordrecht, B. G. Taylor, C. Erd, M. A. C. Perryman, R. Ven, J. Howlett, D. J. Goldie, J. Lumley, and M. Wallis, "Single optical photon detection with a superconducting tunnel junction for potential astronomical use," *Nature*, vol. 381, pp. 135–137, 1996. R. J. Schoelkopf, S. H. Moseley, C. M. Stable, P Wahlgren, and P. Delsing, "A concept for a submillimeter-wave singlephoton counter" *IEEE Trans. Appl. Supercond.*, vol. 9, pp. 2935–2939, 1999.

[12] K. S. Il'in, M. Lindgren, M. Currie, A. D. Semenov, G. N. Gol'tsman, R. Sobolewski, S. I. Cherednichenko, and E. M. Gershenzon, "Picosecond hot-electron energy relaxation in NbN superconducting photodetectors," *Appl. Phys. Lett.*, vol. 76, pp. 2752–2754, 2000.

[13] M. Lindgren, M. Currie, C. Williams, T. Y. Hsiang, P. M. Fauchet, R. Sobolewski, S. H. Moffat, R. A. Hughes, J. S. Preston, and F. A. Hegmann, "Intrinsic picosecond response times of Y-Ba-Cu-O superconducting photodetectors," *Appl. Phys. Lett.*, vol. 74, pp. 853–855, 1999.

[14] A. M. Kadin and M. W. Johnson, "Nonequilibrium photon-induced hotspot: A new mechanism for photodetection in ultrathin metallic films," *Appl. Phys. Lett.*, vol. 69, pp. 3938–3940, 1996.

[15] G. N. Gol'tsman, K. Smirnov, P. Kouminov, B. Voronov, N. Kaurova, V. Drakinsky, J. Zhang, A. Verevkin, and R. Sobolewski, "Fabrication of nanostructured superconducting single-photon detectors," in *these Proceedings*, paper 1EC12.

[16] A. Lipatov, O. Okunev, K. Smirnov, G. Chulkova, A. Korneev, P. Kouminov, G. Gol'tsman, J. Zhang, W. Slysz, A. Verevkin, and R. Sobolewski, "An ultrafast NbN hot-electron single-photon detector for electronic applications," *Supercond. Sci. Technol.*, vol. 15, pp. 1689–1692, 2002.

[17] J. Zhang, W. Slysz, A. Verevkin, G. Chulkova, A. Korneev, A. Lipatov, O. Okunev, G. Gol'tsman, and R. Sobolewski, "Response time characterization of NbN superconducting single-photon detectors," in *these Proceedings*, paper 1EC07.

[18] J. C. Tsang and J. A. Kash, "Picosecond hot electron light emission from submicron complementary metal-oxide-semiconductor circuits," *Appl. Phys. Lett.*, vol. 70, pp. 889–891, 1997.

[19] M. Pavesi, P. L. Rigolli, M. Manfredi, P. Palestri, and L. Selmi, "Spontaneous hot-carrier emission rates in silicon: Improved modeling and applications to metal oxide semiconductor devices," *Phys. Rev. B*, vol. 65, p. 195 209-(1-8), 2002.

[20] G. S. Vernam, "Cipher printing telegraph systems for secret wire and radio telegraphic communications," *J. Amer. Inst. Elec. Eng.*, vol. XLV, pp. 109–115, 1926.

[21] G. Gilbert and M. Hamrick. Practical quantum cryptography: A comprehensive analysis (part one). MITRE Technical Report MTR 0OW0 000 052 (September 2000), to appear in Phys. Rep. [Online]. Available: http://xxx.lanl.gov/abs/quant-ph/0 009 027.

[22] T. R. Clark, T. F. Carruthers, P. J. Matthews, and I. N. Duling, "Phase noise measurements of ultrastable 10 GHz harmonically modelocked fiber laser," *Electron. Lett.*, vol. 35, pp. 720–721, 1999.